Thermal (Kapitza) resistance of interfaces in compositional dependent \(ZnO-In_2O_3\) superlattices

AIP | Applied Physics Letters

Thermal (Kapitza) resistance of interfaces in compositional dependent ZnO-In2O3 superlattices

Xin Liang, Mor Baram, and David R. Clarke

Citation: Appl. Phys. Lett. **102**, 223903 (2013); doi: 10.1063/1.4809784
View online: http://dx.doi.org/10.1063/1.4809784
View Table of Contents: http://apl.aip.org/resource/1/APPLAB/v102/i22
Published by the American Institute of Physics.

Thermal (Kapitza) resistance of interfaces in compositional dependent ZnO-In_2O_3 superlattices

Xin Liang, Mor Baram, and David R. Clarke[a)]
School of Engineering and Applied Sciences, Harvard University, Cambridge, Massachusetts 02138, USA

(Received 1 March 2013; accepted 17 May 2013; published online 7 June 2013)

Compositionally dependent superlattices, $In_2O_3(ZnO)_k$, form in the ZnO-rich portion of the ZnO-In_2O_3 phase diagram, decreasing thermal conductivity and altering both the electron conductivity and Seebeck coefficient over a wide range of composition and temperature. With increasing indium concentration, isolated point defects first form in ZnO and then superlattice structures with decreasing interface spacing evolve. By fitting the temperature and indium concentration dependence of the thermal conductivity to the Klemens-Callaway model, incorporating interface scattering and accounting for conductivity anisotropy, the Kapitza resistance due to the superlattice interfaces is found to be $5.0 \pm 0.6 \times 10^{-10}$ m^2K/W. This finding suggests that selecting oxides with a compositionally dependent superlattice structure can be a viable approach, unaffected by grain growth, to maintaining low thermal conductivity at high temperatures. © *2013 AIP Publishing LLC*. [http://dx.doi.org/10.1063/1.4809784]

Synthetic[1–4] and natural superlattices[5–7] have been reported to exhibit very low thermal conductivities, in some cases close to or even below the minimum thermal conductivity.[8] Compositionally dependent superlattices, sometimes referred to as modular or polysomatic series in the mineralogical literature[9] and homologous series in the crystal chemistry literature,[10] offer the opportunity to select the periodicity of phonon scattering interfaces through choice of composition and thereby the overall thermal conductivity. This possibility has been demonstrated through atomistic simulations of the thermal conductivity of Ruddleston-Popper phases in SrO-$SrTiO_3$ system.[11] Furthermore, as the superlattice spacing is determined by composition, it is expected to be invariant with temperature and not coarsen. This is in contrast to microstructural approaches, such as decreasing grain size and plastic deformation, to decrease thermal conductivity. Over prolonged times at high temperatures these nanostructures coarsen, and their effect on reducing thermal conductivity and increasing ZT in thermoelectrics is lost.

Homologous series form in many oxides, including several semiconducting oxides such as ZnO, Ga_2O_3, and In_2O_3, at high alloying concentrations.[12,13] Many of these oxides are of interest as prospective high-temperature thermoelectrics[14,15] since their electrical conductivity and *ZT* can be modified by aliovalent doping, their thermal conductivity can be modified by altering the superlattice spacing and they are thermodynamically stable to high temperatures. In contrast to synthetic, laboratory-grown superlattices which typically consist of alternating layers of finite thickness and composition, some of these natural superlattices consist of a periodically spaced, single or double atomic layer of one species, such as Sb or In, interleaved within another phase, such as ZnO. Most notable are superlattices in the ZnO-In_2O_3 system.[12,16] In this system, the structure consists of single crystal wurtzite ZnO with single octahedrally coordinated InO_2 sheets lying on the basal plane and separated by a spacing that depends on composition. Notionally, all the phases in this homologous series can be represented by the formula $In_2O_3.(ZnO)_k$, where k is an integer.[17] (With trivalent dopants, such as Fe^{3+}, Ga^{3+}, these ions enter the InO_2 layer extending them into the third dimension in the phase diagram.) Ideally, as represented by the notional formula, the sheets are periodically spaced, but high resolution microscopy reveals that they can often be irregularly spaced.

In this work, we demonstrate that the thermal (Kapitza) resistance of the InO_2 sheets can be derived from the temperature and indium concentration dependence of the thermal conductivity of the indium-doped ZnO. The values of the Kapitza resistance are found to be intermediate between those interfaces in epitaxial semiconductor superlattices and grain boundaries.

Of particular interest is the ZnO-rich portion of the ZnO-In_2O_3 phase diagram.[18] As low concentrations of indium solute are added to ZnO, which is the usual range studied in the electronic doping of ZnO, the solute ion enters the crystal structure at random.[19] With further increases in solute concentration, individual InO_2 sheets form on the basal plane of ZnO and their spacing decreases until, at $x = 0.22$ ($k = 7$), a distinct, identifiable crystallographic compound $Zn_7In_2O_{10}$ forms.[18] So, in essence, a two-phase solid-solution region exists between pure ZnO and $Zn_7In_2O_{10}$ that according to the phase diagram persists up to 1175 °C. (Above this temperature, a different superlattice spacing between the InO_2 sheets becomes stable.[18]) While there remains some uncertainty as to the precise atomic arrangement in this compound, it is known to be rhombohedral (space group $R3\overline{m}$) and the InO_2 sheets are spaced 2.45 nm apart.

The materials studied in this work were bulk, polycrystalline oxides having compositions $(Zn_{1-x}In_x)O$ for indium concentrations, x, over the range $0 \leq x \leq 0.22$. They were prepared by a two-step molecular mixing and combustion process followed by calcination and densification. Specifically, high purity solutions of zinc and indium nitrates

[a)]Author to whom correspondence should be addressed. Electronic mail: clarke@seas.harvard.edu

were mixed with a concoction of arylamindes and persulfate catalyst to form a combustible gel. After drying, the gel was crushed and then heated in a furnace at 600 °C to initiate combustion. The powders were then further calcined at 825 °C for 2 h to remove residual carbon. This wet chemistry method allows a uniform mixture of different ions to form at the molecular level, with the gel-combustion approach freezing the ratio of different types of ions. In combination, these processes give good control of the composition. The powders were then densified into solid pellets 12.7 mm in diameter and 1–1.5 mm in thickness using a current assisted system at 900 °C for 5 min with an applied load of 125 MPa. Following densification, the samples were annealed in air at 900 °C for 2 h to compensate the oxygen deficiency and further post-annealed at 1150 °C for 1 day. To avoid preferential evaporation of In and Zn, the pellets were embedded in oxide powders of the same composition during annealing. The pellets made this way were fully dense and exhibited no preferred crystallographic texture.

The thermal conductivity was determined from thermal diffusivity measurements of the pellets made by the laser flash method[20] (Netzsch LFA 457). Measurements were made from room temperature up to 800 °C in flowing argon gas using a 1.06 μm laser with a (350 μs) pulse. The heat capacities were calculated from the compositions using the Kopp-Neumann rule based on literature data and the mass density measured using Archimedes method. Samples for TEM were made by standard ion-beam milling and samples for atom probe tomography (APT) were prepared by focused ion beam milling and shaping from bulk samples. The atom probe tomography was carried out in a Cameca LEAP 4000X HR microscope using 355 nm pulsed laser excitation.

The measured thermal conductivities as a function of temperature are presented in Figure 1 indicating that the thermal conductivity decreases with increasing indium concentration and also become increasingly less temperature dependent. The lines through the data points correspond to the best fitting using the equations developed below. Figure 2 shows the dependence on indium doping concentration with reference to pure ZnO (made using the same process and post-annealed in air at 1150 °C for 24 h). The figure clearly shows that alloying indium into ZnO significantly reduces its thermal conductivity

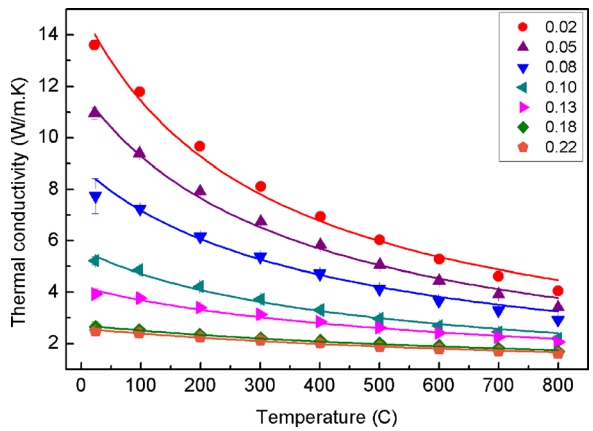

FIG. 1. Thermal conductivity as a function of temperature for the indium concentrations indicated. The solid lines through the data correspond to the Eq. (3) in the text incorporating both point defect and interface scattering.

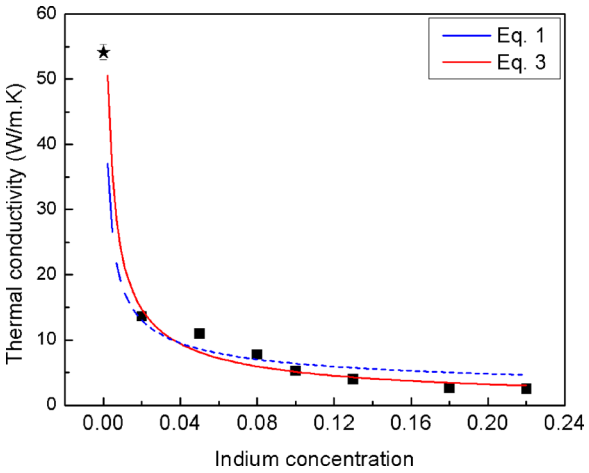

FIG. 2. Room temperature thermal conductivity as a function of indium concentration. The two curves correspond to the Klemens-Callaway model with (Eq. (3)) and without phonon scattering (Eq. (1)) from superlattice compositionally dependent superlattice spacing. The data point represented by $*$ is that of pure, polycrystalline ZnO processed in the same way as the compositions containing indium.

as is expected as a result of solute additions but the reduction does not plateau out as has been reported for other solid-solution systems, such as Si-Ge alloys.[21]

The TEM images illustrate the existence of a superlattice structure, well established in numerous previous publications, for instance.[12,22] Detailed analysis of the superlattice spacings indicates that their spacing averages to that expected from the composition based on individual InO_2 layers interspersed within the ZnO grains. TEM also indicates that no sheets are detectable at indium concentrations below about a composition of $Zn_{0.9}In_{0.1}O$. This is also the concentration at which the lattice parameter abruptly changes with composition (not shown) suggesting the onset of InO_2 sheet formation as distinct from a random solid solution. In all the samples, the average size of the ZnO grains was 2–3 μm, much larger than that at which grain size usually affects thermal conductivity. The APT images, such as Figure 3(b), clearly reveal two important additional features: the indium ions not only form in sheets, as expected, but they are also randomly distributed within the ZnO blocks indicating a co-existing solid solution. In addition, some *Zn* ions are also located within the indium layers. Counting the individual *Zn* and *In* ions recorded and spatially mapping them, indicates that Zn ions are also substituted within the InO_2 sheets and not restricted to the ZnO blocks. (From these and similar images, we cannot determine whether the indium lie in a single or double sheet because of the difficultly in orienting the 3-D reconstruction to the precision necessary. Nevertheless, even if perfectly aligned, the FWHM of the concentration profiles indicates that the interface is no more than 0.7 nm wide, corresponding to a single InO_2 sheet with *In* also having some preference for occupying the adjacent planes of cations on either side.) Taken together, the microscopes indicate that indium ions enter into the ZnO lattice at random and above about $x = 0.1$, they also form a superlattice consisting of quasi-equally spaced InO_2 sheets.

In analyzing the thermal conductivity data, we find that for indium concentrations below about $x = 0.1$, the data are

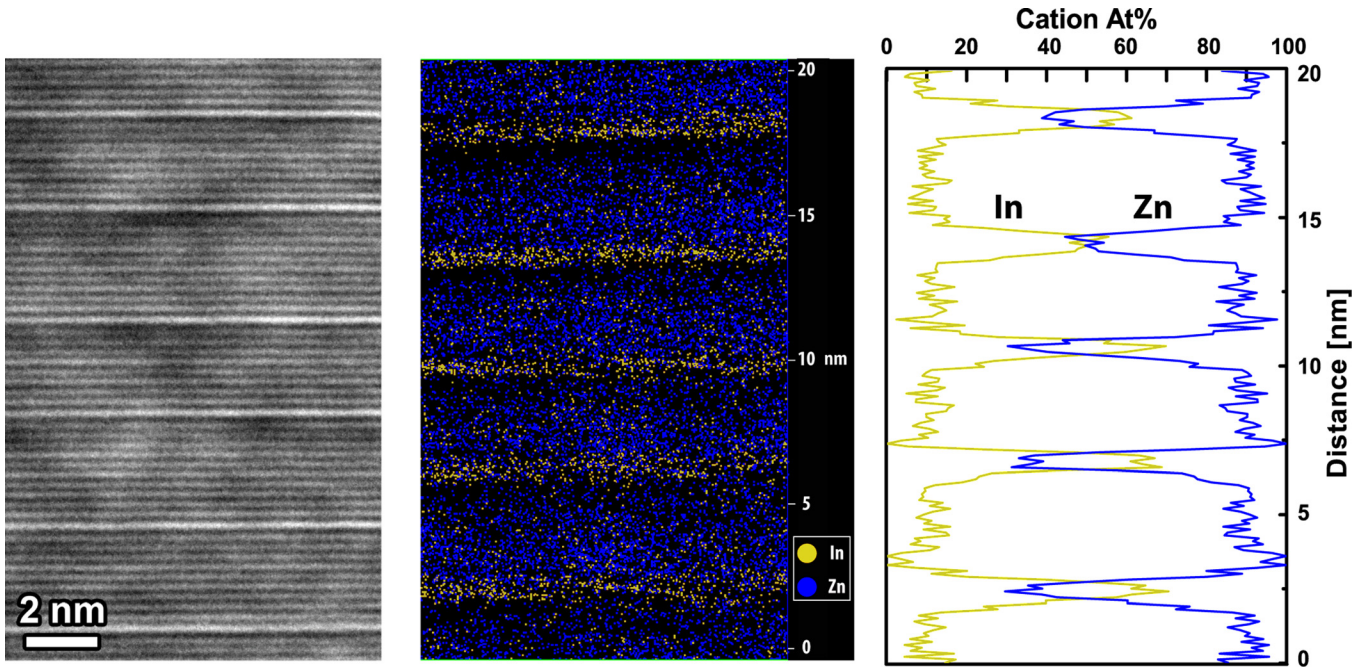

FIG. 3. TEM and APT images of ZnO containing 10% indium ($Zn_{0.9}In_{0.1}O$). The TEM image indicates the presence of an almost periodic superlattice. The APT image (middle) reveals the existence of indium ions in solid solution in the ZnO blocks as well as the indium ions forming irregular InO_2 sheets. The yellow and blue dots represent indium and zinc ions, respectively. (For clarity, the oxygen ions are not shown. Also the magnification is not the same as the TEM image.) The compositional profile (right), obtained from the APT image perpendicular to the superlattice, quantifies the solubility of the indium ions in the ZnO blocks and the zinc ions in the InO_2 sheets.

fully consistent with the Klemens-Callaway model[23] for thermal conductivity of crystals containing defects, incorporating a high-temperature limit, $\kappa_{\min}$. The high temperature limit corresponds to where the phonon wavelengths are equal to the interatomic spacing.[24,25] At high temperature ($T > T_D$) and assuming a Debye spectrum, (the electronic contribution is negligible and ignored in the present study), this relation is given by

$$\kappa_i = \kappa_{min} + \frac{k_B\sqrt{v_s}}{\sqrt{\pi^3}\sqrt{\Omega_0}}\,\frac{1}{\sqrt{\Gamma}}\,\frac{1}{\sqrt{C\,T}}\,tan^{-1}\left(\frac{k_B T_D}{\hbar}\left(\frac{\Omega_0\,\Gamma}{4\pi {v_s}^3\,C\,T}\right)^{\frac{1}{2}}\right), \quad (1)$$

where k_B is Boltzmann's constant, v_S the sound velocity of ZnO (4008 m/s (Ref. 26)), Ω_0 the unit cell volume (4.762×10^{-29} m^3), T_D the Debye temperature (370 K for ZnO[26]), and the constant C is the inverse time coefficient for phonon-phonon scattering processes in pure, un-doped ZnO.[23] Γ is the phonon scattering strength of point defects formed by indium solid solution alloying and depends on the mass variance due to doping at each atomic site. It is well established from computational and crystal chemical studies[27] that as indium ions are added to ZnO, they substitute onto the cation sites and are accompanied by the formation of cation vacancies (one for every two indium ions) to maintain charge neutrality. Consequently, the only defects that can cause phonon scattering are mass disorders associated with indium atoms and associated cation vacancies. The phonon scattering factor is then given by the sum of the mass variance[28] on the Zn site due to the presence of indium and vacancies on that site,

$$\Gamma = x\,\frac{(M_{In} - \overline{M}_{ZnO})^2}{2\,(\overline{M}_{ZnO})^2} + \frac{x}{2}\,\frac{(\overline{M_{Zn}})^2}{2\,(\overline{M}_{ZnO})^2}, \quad (2)$$

where $\overline{M}_{ZnO}$ is the mean mass of the In-doped ZnO formula unit. To first order in indium concentration, x, and up to $x = 0.22$, Γ is given by: $\Gamma \cong 1.38\,x$. The constant, C, found by fitting the temperature dependence of pure, polycrystalline ZnO from 300 K to 1273 K, was found to have a value of 1.3×10^{-18} (R-square value of 0.99).

For indium concentrations greater than about $x = 0.1$, the fit of the Klemens-Callaway model to the data becomes progressively poorer as the indium concentration is increased. As this is the compositional range over which microscopy reveals that distinct superlattice interfaces form, we conclude that the InO_2 sheets also scatter phonons and further reduce the thermal conductivity. The superlattice sheets can be expected to introduce a thermal conductivity anisotropy so that the conductivity perpendicular to the sheets, κ_z, is different than the conductivity, $\kappa_x = \kappa_y$, parallel to them. (This latter in-plane conductivity, κ_x, is the same as the intrinsic conductivity, κ_i, introduced above to describe due to solute scattering.) Assuming the contribution to thermal conductivity perpendicular to the sheets is as a thermal resistance in series with the In-doped ZnO blocks given by Eq. (1), the additional thermal resistance can be expressed as a Kapitza resistance, R_k,

$$\frac{1}{\kappa_z} = \frac{1}{\kappa_i} + \frac{R_k}{d_{SL}} = \frac{1}{\kappa_i} + \frac{R_k}{(k+1)\,d_{\{0002\}}}, \quad (3)$$

where d_{SL} is the average interface spacing, which, in turn, depends on the indium concentration according to the relationship,

TABLE I. Examples of interfacial thermal resistances.

Material	Interface type	Kapitza resistance (10^{-10} m^2 K/W)	Temperature range, K	Reference
ZnO-In_2O_3	Superlattice	5.0	RT to 1073	This work
Si/Ge	Epitaxial superlattices	4.0	200	Lee[4]
AlN/GaN	Epitaxial superlattices	5–16	RT	Koh *et al.*[3]
W/alumina	Nanolaminate	31.3	RT	Costescu *et al.*[8]
Ni/Ti	Nanolaminate	19	RT	Clemens *et al.*[2]
Ni/Zr	Nanolaminate	23	RT	Clemens et al
Si	Grain boundaries	13	80–400 K	Cahill[34]
$SrTiO_3$	Grain boundaries	49.8–34.1	300–1000	Wang *et al.*[32]
YSZ	Grain boundaries	45	373–1273	Limarga *et al.*[33]

$$d_{SL} \approx (k+1) \times d_{\{0002\}}, \tag{4}$$

where $d_{\{0002\}}$is the ZnO basal plane spacing (0.260 nm). (This macroscopic model[29] is used rather than the microscopic phonon model incorporating interfaces since otherwise there are so many fitting parameters that there are multiple combinations of parameters that will fit the data.) As discussed by Mityushov *et al.*,[30] and more recently elaborated upon in Yang *et al.*,[31] the effect of crystallographic thermal anisotropy in polycrystalline materials containing randomly oriented, superlattice grains can be represented in terms of the conductivity anisotropy, $r = \kappa_z/\kappa_x$, by the

$$\frac{\kappa^*}{\kappa_x} = \frac{r+2}{3} - \frac{2}{9}\frac{(r-1)^2}{(r+2)}, \tag{5}$$

where κ^* is the measured conductivity of the bulk, polycrystalline material as a function of indium concentration. When the Kapitza resistance of the superlattice interfaces is included to introduce a compositionally dependent conductivity anisotropy, given by Eqs. (3)–(5), the calculated thermal conductivity fits both the temperature and composition dependence extremely well as shown in Figures 1 and 2.

The value of the Kapitza resistance derived from fitting Eqs. (1)–(5) to the experimental data, $5.0 \pm 0.6 \times 10^{-10}$ m^{2}K/W, is comparable to those of epitaxial semiconductor interfaces (Table I), and is also substantially smaller than grain boundaries in $SrTiO_3$[32] and in yttria-stabilized zirconia[33] (both above their respective Debye temperatures), as well as interfaces in metallic nanolaminates. The temperature independence of the Kapitza resistance is consistent with the values reported for grain boundaries above room temperatures.[32,33] While no physical model adequately predicts the value of the Kapitza resistance for a single atomic layer interface, it is reasonable that our measured value is comparable to an epitaxial interface since the lattice is continuous across the superlattice interface apart from a possible lattice inversion when the sheet corresponds to an inversion layer boundary. Furthermore, the thermal conductivity model incorporating the interface scattering adequately represents that of the single phase, end member, $Zn_7In_2O_{10}$, (x = 0.22) as well as across the entire solid solution range, suggesting that the thermal conductivity can be well described by the series conductances of the superlattice interfaces together with solid solution point-defect scattering.

In conclusion, we observe that with increasing doping concentration, the microstructure of indium-doped ZnO evolves from isolated point defects to a combination of point defects and superlattice structures with decreasing interface spacing. It is also found that indium ions are present in solid solution in the ZnO blocks even when superlattice structure forms. Using this information, the thermal conductivity is fully described as a function of temperature (above room temperature) and concentration by the Klemens-Callaway model incorporating a Kapitza resistance of $5.0 \pm 0.6 \times 10^{-10}$ m^{2}K/W for the scattering from the individual superlattice interfaces. This suggests that homologous series of compounds may be attractive, coarsening-resistant candidates in the search for high-temperature thermoelectrics.

[1]R. M. Costescu, M. A. Wall, and D. G. Cahill, Phys. Rev. B **67**, 054302 (2003); D. Josell, A. Cezairliyan, and J. E. Bonevich, Int. J. Thermophys. **19**(2), 525 (1998).
[2]B. M. Clemens, G. L. Eesley, and C. A. Paddock, Phys. Rev. B **37**(3), 1085 (1988).
[3]Y. K. Koh, Y. Cao, D. G. Cahill, and D. Jena, Adv. Funct. Mater. **19**(4), 610 (2009).
[4]S. M. Lee, D. G. Cahill, and R. Venkatasubramanian, Appl. Phys. Lett. **70**(22), 2957 (1997).
[5]Y. Shen, D. R. Clarke, and P. A. Fuierer, Appl. Phys. Lett. **93**, 102907 (2008).
[6]T. D. Sparks, P. A. Fuierer, and D. R. Clarke, J. Am. Ceram. Soc. **93**(4), 1136 (2010).
[7]C. L. Wan, T. D. Sparks, P. Wei, and D. R. Clarke, J. Am. Ceram. Soc. **93**(5), 1457 (2010).
[8]R. M. Costescu, D. G. Cahill, F. H. Fabreguette, Z. A. Sechrist, and S. M. George, Science **303**, 989 (2004).
[9]D. R. Veblen, Am. Mineral. **76**(5–6), 801 (1991).
[10]R. J. D. Tilley, *Crystals and Crystal Structures* (Wiley, Hoboken, 2008).
[11]A. Chernatynskiy, R. W. Grimes, M. A. Zurbuchen, D. R. Clarke, and S. R. Phillpot, Appl. Phys. Lett. **95**, 161906 (2009).
[12]P. J. Cannard and R. J. D. Tilley, J. Solid State Chem. **73**, 418 (1988).
[13]N. Kimizuka and T. Mohri, J. Solid State Chem. **78**(1), 98 (1989); N. Kimizuka, E. Takayama, and K. Siratori, in *Handbook on the Physics and Chemistry of Rare Earths*, edited by K. A. Gschneidner, and L. Eyring (North-Holland, Amsterdam, 1990), Vol. 13, p. 283.
[14]Xin Liang, Ph.D. Dissertation, Harvard University, 2013.
[15]H. Ohta, W.-S. Seo, and K. Koumoto, J. Am. Ceram. Soc. **79**, 2193 (1996).
[16]M. Nakamura, N. Kimizuka, and T. Mohri, J. Solid State Chem. **93**, 298 (1991).
[17]N. Kimizuka, M. Isobe, and M. Nakamura, J. Solid State Chem. **116**, 170 (1995).
[18]T. Moriga, D. D. Edwards, T. O. Mason, G. B. Palmer, C. R. Poeppelmeier, J. L. Schindler, C. R. Kannewurf, and I. Nakabayashi, J. Am. Ceram. Soc. **81**(5), 1310 (1998).
[19]A. Janotti and C. G. Van der Walle, Rep. Prog. Phys. **72**, 126501 (2009).
[20]W. J. Parker, R. J. Jenkins, C. P. Butler, and G. L. Abbott, J. Appl. Phys. **32**(9), 1679 (1961).
[21]B. Abeles, D. S. Beers, G. D. Cody, and J. P. Dismukes, Phys. Rev. **125**(1), 44 (1962).

[22]Y. Yan, S. J. Pennycook, J. Dai, R. P. H. Chang, A. Wang, and T. J. Marks, Appl. Phys. Lett. **73**, 2585 (1998).
[23]J. Callaway and H. C. von Baeyer, Phys. Rev. **120**(4), 1149 (1960).
[24]M. C. Roufosse and P. G. Klemens, J. Geophys. Res. **79**(5), 703, doi:10.1029/JB079i005p00703 (1974).
[25]D. G. Cahill, S. K. Watson, and R. O. Pohl, Phys. Rev. B **46**(10), 6131 (1992).
[26]R. A. Robie and J. L. Edwards, J. Appl. Phys. **37**(7), 2659 (1966).
[27]M. A. McCoy, R. W. Grimes, and W. E. Lee, Philos. Mag. A **76**(6), 1187 (1997).
[28]R. Berman, E. L. Foster, and J. M. Ziman, Proc. R. Soc. London Ser. A **237**(1210), 344 (1956).
[29]C. W. Nan and R. Birringer, Phys. Rev. B **57**(14), 8264 (1998); C. W. Nan, R. Birringer, D. R. Clarke, and H. Gleiter, J. Appl. Phys. **81**(10), 6692 (1997).
[30]E. A. Mityushov, R. A. Adamesku, and P. V. Gel'd, J. Eng. Phys. **47**(3), 1052 (1984).
[31]F. Yang, T. Ikeda, G. J. Snyder, and C. Dames, J. Appl. Phys. **108**(3), 034310 (2010).
[32]Y. Wang, K. Fujunami, R. Zhang, C. L. Wan, N. Wang, Y. Ba, and K. Koumoto, Appl. Phys. Express **3**, 031101 (2010).
[33]A. M. Limarga and D. R. Clarke, Appl. Phys. Lett. **98**, 211906 (2011).
[34]D. G. Cahill, M. Katiyar, and J. R. Abelson, Phys. Rev. B **50**, 6077 (1994).